Geosci. Instrum. Method. Data Syst. Discuss., https://doi.org/10.5194/gi-2018-27
Manuscript under review for journal Geosci. Instrum. Method. Data Syst.
Discussion started: 2 January 2019

Geoscientific Instrumentation Methods and Data Systems Discussions

A full waveform current recorder for electrical prospecting

Kai Chen, Sheng Jin

China University of Geosciences, Beijing, 100083, China

Correspondence to: Kai Chen (ck@cugb.edu.cn)

Abstract: Current data is an important input data for electrical prospecting data post-processing. Presently, the current recorder has deficient capability for continuous recording, precision, bandwidth, dynamic range, and input range. A new full waveform current recorder for measuring current signal that is ideal for electrical prospecting applications is presented. The new measurement principle enables the fabrication of a high precision current sensor with an autonomous data logger as well as continuous measuring capabilities for full waveforms that are comparable to recent developments for electrical prospecting applications. The full waveform current recorder is capable of measuring current with bandwidth from DC to 10 kHz, with a power spectrum density noise floor of 10 μA/rt(Hz) at 10 Hz. The current recorder has a dynamic range that is higher than 97 dB over a range of 100 A at peak, with time synchronization error as low as ±0.1 μs. All of these features make current measurement a promising technology for high precision measurement with long duration, autonomous data logging for field electrical prospecting applications.

Keywords: full waveform current measurement, electrical prospecting, autonomous data logger, current probe

1 Introduction

Electrical prospecting contains many branch methods, such as time-domain induced polarization (TDIP) (Fiandaca et al., 2012), spectral induced polarization (SIP) (Vanhala, 2010), direct-current resistivity (DCR) (Monteiro et al., 2011), magnetotellurics (MT) (Cagniard, 1953), and controlled source electromagnetic surveying (CSEM) (Boerner et al., 1993), which have been successfully applied on mineral exploration, hydrocarbons prospecting, and ground water investigation.

At present, CSEM sounding measurements are mostly interpreted by their apparent resistivity. In far zone sounding, the electric field and the magnetic field components are proportional to the electron magnetic moment of the controlled source, and therefore, the effect of the field source parameters on resistivity can be ignored in the case of far zone sounding. However, when a single component (E-field or B-field) is used to calculate a normalised field, the current data must be calculated for data post-processing. This requires the current signal to be recorded with high precision (Constable, 2013). For TDIP applications, owing to the variable grounding resistance in field conditions, the load of the transmitter is not stable, and the real current amplitude is not a constant. To get the high-precision resistivity result required, the precision of current amplitude measurement should be ensured. For SIP applications, complex resistivity is calculated by current data, measuring both phase

and amplitude, so achieving a low time synchronization error for current measurement is important. For the application of the controlled source audio magnetotelluric (CSAMT) method (Boerner et al., 1993a), the current is not used as the input for data post-processing, but the current data can provide a reference for the evaluation of the transmitter quality. Furthermore, when the transmitter launches a pseudo-random sequence (PRS) (Ramayya et al., 2008), the pulse width is narrow, not only measuring current amplitude, but also requiring broader sampling bandwidth and time precision.

As shown in the preceding examples, current is an important parameter for data post-processing in electrical prospecting. In order to meet the above requirements, current recorders focus on full waveform recording, bandwidth, amplitude accuracy, and time precision.

Instruments were recently developed to measure current for advanced electrical prospecting, such as the RXU-TMR from Phoenix Geophysics (PhoenixGeophysics, 2018) and the I-FullWaver from IRIS (IRIS, 2018). A comparison of performance among various current recorders is shown in Table 1. To meet requirements for current measurement in high power multifunction transmitters, which use PRS waveform and broad bandwidth CSEM, there is some deficiency for input range, precision, bandwidth, and continuous recording. The I-FullWaver is designed for TDIP, and its bandwidth is limited. The RXU-TMR from Phoenix is suitable for CSAMT, TDIP, and SIP, but the raw data is discontinuous and therefore not suitable for PRS applications. Zhang et al. (2017) developed a full-waveform voltage and current recording device for multi-transient electromagnetic (MTEM) (Ziolkowski et al., 2010) applications, with continuous recording capability, but the accuracy and dynamic range are limited. Furthermore, its current transducer is based on sample resistance, which is lackluster for galvanic isolation.

Considering the above analysis, an acceptable current recorder should have the following characteristics: 1) The input range that is suitable for a high-power multifunction transmitter. 2) Acceptable precision for measurement of amplitude. 3) Accurate and consistent time synchronisation while recording current to decrease the phase calculation error. 4) Continuous current sampling and full waveform recording for current amplitude and phase variable. In short, the development of current recorders mainly focuses on the accuracy of amplitude, the accuracy of time synchronisation, sufficient bandwidth, and continuous recording at a sufficient input range for full waveform recording.

2 Method

2.1 Design overview

Current information is required for deconvolution calculations for post-processing. The current waveform recorder for current signals is a new device concept designed for SIP, TDIP, and advanced CSEM sounding. It can work in all field conditions, as it is compact, efficient, discrete, and can autonomously record full, continuous current waveforms. This current recorder uses a Hall effect sensor to accurately measure and log the injected current I_{AB} by proximity, without requiring direct contact. The

current recorder is connected close to the transmitter or any injection, and an internal GPS that accurately provides a pulse per second (PPS) signal allows the device to store a continuous series with high precision time stamping, which is crucial to the correlation and processing of data from an EM receiver installed nearby. The measurement of I_{AB} is used to evaluate the behaviour of the transmitter and to accurately compute the apparent resistivity. Current samples are recorded at a sample rate of either 24 kHz or 2400 Hz, and all raw data is synchronised through the GPS-PPS time stamping. Post-acquisition data processing improves the signal-to-noise ratio (SNR) for better results regarding data quality due to the highly precise nature of current information, allowing for deeper investigations in the case of noisy areas.

The current recorder continuously saves time series records of its output current on a removable flash memory SD card. The full waveform current recorder contains an integrated class 10 32 GB SD card for storage, and can store up to 90 h of data, corresponding to 11 eight-hour working days, with a 24 kHz sampling rate. Alternatively, the data on the flash memory card can be uploaded to the post-processing computer via a high-speed Ethernet interface in the field at a maximum transfer rate of 10 MB/s.

When the transmitter is working in the field, the current recorder performs measurement using a built-in current probe. While the current probe is engaged with the cable, the probe's output voltage is linear with current in the cable based on the Hall effect. Fig. 1 presents the system work principle. The multifunction EM transmitter contains a high-power diesel generator, a high-power AC/DC regulator, a chopper module, a data acquisition unit, a current probe, two long-distance cables, two electrode plates, and an external tablet computer (PAD).

2.2 Hardware principle

The current recorder contains the current probe and the data acquisition unit. Fig. 2 presents the diagram of the current recorder. The data acquisition unit consist of a GPS antenna, an allium box, five printed circuit boards (PCB), and a built-in battery. The PCB contains a front interface module, an Analog-to-Digital Converter (ADC) module, a Field-Programmable Gate Array (FPGA) module, an Advance RISC Machine (ARM) module, a clock module, and a power module. The front interface module integrates protection of the input circuit and anti-aliasing filter, with connectors inside and outside the allium box. The NET interface is used to communicate with the external user PAD. The ADC module amplifies the voltage signal from the current probe output and converts that signal to a serial digit output. The sample rate is set as either 24000 Hz or 2400 Hz. The bandwidth is set as either 10 kHz or 1 kHz. The FPGA module reads the data stream and adds the GPS time stamp, and the ARM module transfers data from the FPGA to the built-in SD card. The CLK module provides GPS time information and PPS for the ARM and FPGA modules. Each discrete module is integrated by bus. The power module converts the Li-ion battery voltage to analog and digital power sources. The capacity of the battery is 20 Ah at 12 V, and the whole power consumption is about 6 W. Maximum working time is about 40 h, which is enough for field work. Fig. 3 shows the photo of the data acquisition unit.

The current recorder not only provides continuous real-time acquisition, but also transfers data to the PAD for raw time series display. Fast Ethernet is used to transfer data between the current recorder and the PAD, which is a Microsoft Surface 2 running Windows RT OS. The PAD configures the acquisition parameters and displays the waveform time series in real time. The acquisition parameter includes the sample rate and sensitivity of the current probe, as well as other values. The parameter configuration function is accessed using the Telnet protocol, and the time series data transfer is performed using UDP. Although the display data is not continuous, the data stored on the SD card is continuous. While the sample rate set at 24 kHz, the data throughput rate is 4 B/ch*24 kHz = 96 KB/s, for a total data store rate of about 338 MB per hour. The Fast Ethernet (100 Mbps) is sufficient to reach the data transfer requirement. For an eight-hour working day, the total data volume may reach 2.7 GB per day. The SD storage space is 32 GB, which is enough for 90 h (about 11 eight-hour working days).

Time synchronization is another key specification. Fig. 4 presents the diagram of the clock module, which contains an LEA-6T GPS made by u-blox, FPGA, Oven Controlled Crystal Oscillator (OCXO) made by KVG Inc., and Digital-to-Analog converter (DAC). The GPS module provides high precision time source with PPS drift error as low as 20 ns. The output frequency of the OCXO is set as 12.288 MHz, with 10 ppb frequency stability in over temperature range. Before the data acquisition unit is started, the FPGA must calibrate the output clock of OCXO CLK_OCXO using the PPS. The FPGA generates another PPS_local signal output as local PPS which divide from the OCXO, FPGA measure the time different between the PPS_GPS from GPS and the PPS_local real time, when the gap exceeds 0.1 μs, the FPGA adjust the taming voltage Vc of the OCXO by DAC output for calibrating the OCXO output frequency.

2.3 Current probe

In the current measurement application, an available current transducer can be selected from sample resistance, inductance mutual, Hall effect sensor, and fibre sensor. Table 2 presents a comparison of different sensors for current measurement. Considering bandwidth, galvanic isolation between the primary and secondary circuits, precision, input range, and cost, the Hall effect sensor is the best choice for a full waveform current recorder.

After evaluation and investigation, the Tektronix A622(Tektronix 2018) was selected as the current sensor. This is a Hall effect current sensor, and meets the requirements of bandwidth, input range, precision and compact design. Table 3 presents the main specifications of the A622. This ‘long nose’ style clamp-on probe uses a Hall effect current sensor to provide a voltage output linearity with the input current to data acquisition unit. It has a BNC connector and can be used with a shrouded banana plug adapter, so it can also be used on digital multimeters, TekMeter devices, and oscilloscopes. The A622 can measure AC/DC currents from 50 mA to 100 A peak over a frequency range of DC to 100 kHz. It provides 10 mV or 100 mV output for each Amp measured.

Geosci. Instrum. Method. Data Syst. Discuss., https://doi.org/10.5194/gi-2018-27
Manuscript under review for journal Geosci. Instrum. Method. Data Syst.
Discussion started: 2 January 2019

Geoscientific Instrumentation Methods and Data Systems Discussions
Open Access
EGU

2.4 Software principle

The software contains an ARM-Linux driver and an ARM-Linux application that is built on the Embedded Linux platform, PAD-Windows application run in Windows OS build by Visual C++. Fig. 5 present the data flow chart of the current recorder. The flow chart can divide two part: up flow and down flow. Down flow, user configure the data acquisition parameter (gain, sample rate, etc.) by application on PAD, and PAD send the parameter file to ARM platform by telnet protocol, ARM-Linux application analyse the parameter file and configure the ADC by FPGA. Up flow, ARM-Linux application read the converted data from ADC by FPGA, and write the data to SD card, furthermore send to PAD by UDP protocol. To ensure the recording of continuous data, the direct memory access (DMA) in ARM was used for data transfer, and multiple threads were created for read FPGA, write SD files, and send UDP data frames to the PAD. The ARM-Linux application was used as a server, and the PAD-Windows application was used as a client.

Due to the high sampling rate, current files are saved in binary mode in order to save disk space. For high throughput data transfer and local file saving, the current acquisition application is installed on the ARM-Linux platform with the high efficiency user application software on PAD, fast Ethernet, and high-class SD card. The Linux driver used for data acquisition depends on Ping-Pong principle which is designed for data block transfer between kernel and application and DMA hardware, so data may be saved to SD with a high throughput data rate and no missing data.

The above software and hardware platform has been verified with four-channel 24 kHz sample rate continuous data acquisition and the data throughput rate reach 388 KB/s. the high data throughput rate principle provides enough data throughput rate for the current recorder.

3 Test

3.1 Laboratory test

Laboratory tests were conducted for time sync error, input range, self-noise level, dynamic range, and bandwidth specification. The following method was used to measure the noise level of the current probe and the data acquisition unit. Firstly, shorted the input of data acquisition unit, and record the noise time series to measure the self-noise power spectrum density of the data acquisition unit channel. Secondly, with the current probe placed on a magnetic shield barrel, the sensitivity of the current probe set as 100 mV/A, and the data acquisition unit sample set as 24 kHz, we calculated the noise power spectrum density. As shown in Fig. 6, the current noise power spectrum density of channel and probe was about 10 μA/rt (Hz)@10 Hz. The dynamic range was about 97 dB with 10 kHz bandwidth.

The data acquisition integrated 24 bits ADC, and the dynamic range reached 100 dB with 10 kHz band width. The bandwidth of the A622 current probe reached 100 kHz, and with bandwidth of the data acquisition set as DC to 10 kHz, the sample rate was set as 24 kHz. The maximum transmission current of the high-power transmission system studied by the research group

can reach 60 A, while the input range of the current probe set as 100 A.

3.2 Field experiment

To evaluate the performance of the full waveform current recorder in field conditions, we conducted field ore exploration experiments on Linxi county, which is in Northern China. 15 EMR6 EM receivers (Chen et al., 2017) and two EMT48 multifunction transmitters (Wang et al., 2017) were deployed for field work. The EM receivers and transmitters were set as multifunction, which supports many electrical prospecting methods, such as TDIP, SIP, CSAMT, and PRS mode data acquisition.

As the most advanced controlled current source available for electrical prospecting exploration, the EMT48 incorporates many of the features of the ground-breaking new technology developed in 2016 for the 48 kW chopper unit. The chopper module is a compact portable model, combining substantial power output with great reliability, flexibility, and user-friendly operation.

For CSAMT mode, the circular frequency list is from 9600 Hz to 0.9375 Hz, lasting 50 min. The circular frequency list contains 41 frequency points, with the duration of each frequency point set between 40 s and 300 s against the frequency variable. The distance between the transmitter and the receiver is about 6 km. The transmitter dipole length is 1300 m, and the contacted ground resistance is approximately 30 Ω. When transmitter voltage is set as 900 V and transmitter output frequency is set as 120 Hz, the output current reaches 30 A at peak. While the transmitter is operational, the current recorder measures the current continuously. Fig. 7a presents the raw time series, which lasts about 20 min in a circular list. Fig. 7b presents the frequency stack result. The transmit circular list cycles from high frequency to low frequency, and in the high frequency band, the amplitude of current is low due to resistance induced by cable length. The minimum current is as low as 2 A and the maximum current is approximately 30 A. In the low frequency band, the main source of ground resistance is the earth resistance, and the induced resistance from cable length is negligible. The corner frequency is about 2000 Hz. The time frequency spectrum (Marple, 2002) result presents the current frequency variable over time, and the colour bar presents the current amplitude variable as frequency. Fig. 7c illustrates the full spectrum of each frequency waveform time series from 300Hz to 0.09375Hz. The amplitude of high band frequency is lower than the low band frequency, and the duration is shorter than the low band frequency. The harmonic of the fundamental frequency is obvious due to the square waveform.

In SIP method mode, the circular frequency list duration is 15 min, ranging from 128 Hz to 1/16 Hz. It contains 12 frequency points, for which each frequency point duration ranges from 50 s to 270 s. The length of the transmitter dipole is 25 m, and the distance between the transmitter and the receiver is 75 m. Due to the short distance between the transmitter and the receiver, the SNR and total E-field are large, and the current amplitude is set as 2 A peak. While the transmitter is working, the current recorder acquires data continuously. Fig. 8a presents the raw current time series and time frequency spectrum. During the circulation frequency list, the amplitude of current is almost constant, at about 2 A. Fig. 8b presents the time frequency spectrum of the output current. The result displays the frequency step schedule from 128 Hz to 1 Hz.

In TDIP mode, positive zero negative zero (PZNZ) waveform was generated by the transmitter. The source dipole length is 1600 m, and the amplitude current is approximately 15 A peak. The pulse width lasted four seconds, and the whole period lasted 16 seconds. Fig. 9a presents the current amplitude variable in a working day lasting 8 h. The transmitter started at AM 8:40, and from AM 8:40 to AM 9:10, the current was about 5 A for the purpose of status verification for the transmitter being operational. After the operational status verification procedure, the current was increased to 15 A until 09:20, stopping at 14:00. During these 5 h, the amplitude increases from 14.5 A to 15 A due to the grounding contact resistance decline.

From the results of the above experiment, Table 4 presents the comparison of the specifications of the developed full waveform recorder and Phoenix transmitter control unit (TMR-RXU), which integrated the current measurement function. The developed full waveform recorder is a better data logger for the multifunction EM transmitter for electrical prospecting applications.

4 Conclusion

The performance of the existing current recorder is deficient with regard to advanced electrical prospecting requirements for full waveform continuous acquisition. The new developed full waveform current recorder described in this paper was found to be useful for multifunction EM transmitters for electrical prospecting. The field experiment results of the experiment show that the full waveform recorder could autonomously measure current in field conditions. The raw current time series presents the detail of the transmitter output current waveform, providing high precision amplitude and phase information for data post-processing. The continuous series is recorded for calculation as a stack. In TDIP mode, the low variation of current amplitude is given. In CSAMT mode, the time frequency spectrum result displays the current amplitude decreasing as the frequency increases. The current waveform had the additional advantages of ease of use and low power consumption.

In our future research, high-power voltage information from the chopper module output can be measured identically to the current information using a galvanic isolated voltage attenuator. The channel and storage space has been reserved, and effective data throughput technology is available.

Author Contributions

Kai Chen developed the required hardware and software. Sheng Jin created the overall design and performed the experiment.

Competing Interests

The authors declare that they have no conflict of interest.

Acknowledgements.

General funding was provided by the National High Technology Research and Development Program of China (2014AA06A603, 2016YFC0303100, 2017YFF0105700) and National Science Foundation of China (41804071, 61531001).

References

Boerner, D. E., R. D. Kurtz, and A. G. Jones.: Orthogonality in CSAMT and MT measurements. Geophys., 58 (7), 924–934, 1993a.

Boerner, D. E., J. A. Wright, J. G. Thurlow, and L. E. Reed.: Tensor CSAMT studies at the Buchans Mine in central Newfoundland. Geophys., 58 (1), 12–19, 1993b.

Cagniard, L.: Basic theory of the magneto-telluric method of geophysical prospecting. Geophys., 18 (3), 605–635, 1953.

Chen, K., S. Jin, and S. Wang.: Electromagnetic receiver with capacitive electrodes and triaxial induction coil for tunnel exploration. Earth Planets & Space, 69(1),123, 2017.

Constable, S. C.: Review paper: Instrumentation for marine magnetotelluric and controlled source electromagnetic sounding. Geophysical Prospecting, 61, 505–532, doi: 10.1111/j.1365-2478.2012.01117.x, 2013.

Fiandaca, G., E. Auken, A. V. Christiansen, and A. Legaz.: Time domain induced polarization. Geophys., 77(3), 213, 2012.

IRIS. I-FullWaver 2018. Available from http://www.iris-instruments.com/i-fullwaver.html.

Marple, S. L., Jr.: Computing the discrete-time “analytic” signal via FFT. IEEE Trans. Sig. Process., 47(9),2600-2603, 2002.

Monteiro Santos, F. A., and H. M. Elkaliouby.: Quasi-2D inversion of DCR and TDEM data for shallow investigations. Geophys., 76 (4) 4, F239, 2011.

PhoenixGeophysics. 2018, V8 RECEIVER 2018 [cited 1-Jan 2018]. Available from http://www.phoenix-geophysics.com/products/receivers/v8/?

Ramayya, B. Dasaradha, R. Prasad, Tadepalli, Rao, and Y. Purnachandra.: A process and device for measurement of spectral induced polarization response using Pseudo Random Binary Sequence (PRBS) current source. U.S. Patent, 2002.

Tektronix. A621&A622 current probe 2018. Available from https://www.tek.com.cn/datasheet/a621-a622-current-probes-datasheet.

Vanhala, H.: Mapping Oil-Contaminated Sand and Till With the Spectral Induced Polarization (Sip) Method. Geophys. Prospecting, 45 (2), 303–326, 2010.

Wang, M., S. Jin, M. Deng, W. Wei, and K. Chen.: Multi-function electromagnetic transmitting system for mineral exploration. IEEE Trans. on Power Electron., PP (99), 1–1, 2017.

Zhang, X., Q. Zhang, M. Wang, Q. Kong, S. Zhang, R. He, S. Liu, S. Li, and Z. Yuan.: Development of a full-waveform voltage and current recording device for multichannel transient electromagnetic transmitters. Geoscientific Instrumentation Methods & Data Systems, 6(2), 1–13, 2017.

Ziolkowski, A., R. Parr, D. Wright, V. Nockles, C. Limond, E. Morris, and J. Linfoot.: Multi-transient electromagnetic repeatability experiment over the North Sea Harding field & Dagger. Geophysical Prospecting, 58 (6), 1159–1176, 2010.

Boerner, D. E., R. D. Kurtz, and A. G. Jones. 1993a, Orthogonality in CSAMT and MT measurements. Geophysics, **58**, no. 7,924-934.

Boerner, D. E., J. A. Wright, J. G. Thurlow, and L. E. Reed. 1993b, Tensor CSAMT studies at the Buchans Mine in central Newfoundland. Geophysics, **58**, no. 1,12-19.

Cagniard, L. 1953, Basic theory of the magneto-telluric method of geophysical prospecting. Geophysics, **18**, no. 3,605-635.

Chen, K., S. Jin, and S. Wang. 2017, Electromagnetic receiver with capacitive electrodes and triaxial induction coil for tunnel exploration. Earth Planets & Space, **69**, no. 1,123.

Constable, S. C. 2013, Review paper: Instrumentation for marine magnetotelluric and controlled source electromagnetic sounding. Geophysical Prospecting, **61**,505-532. doi: 10.1111/j.1365-2478.2012.01117.x.

Fiandaca, G., E. Auken, A. V. Christiansen, and A. Legaz. 2012, Time Domain Induced Polarization. Geophysics, **77**, no. 3,213.

IRIS. I-FullWaver 2018. Available from http://www.iris-instruments.com/i-fullwaver.html.

Marple, S. L., Jr. 2002, Computing the discrete-time "analytic" signal via FFT. IEEE Transactions on Signal Processing, **47**, no. 9,2600-2603.

Monteiro Santos, F. A., and H. M. Elkaliouby. 2011, Quasi-2D inversion of DCR and TDEM data for shallow investigations. Geophysics, **76**, no. 4,F239.

PhoenixGeophysics. 2018, V8 RECEIVER 2018 [cited 1-Jan 2018]. Available from http://www.phoenix-geophysics.com/products/receivers/v8/?

Ramayya, B. Dasaradha, R. Prasad, Tadepalli, Rao, and Y. Purnachandra. 2008, A process and device for measurement of spectral induced polarization response using Pseudo Random Binary Sequence (PRBS) current source.

Tektronix. A621&A622 current probe 2018. Available from https://www.tek.com.cn/datasheet/a621-a622-current-probes-datasheet.

Vanhala, H. 2010, MAPPING OIL-CONTAMINATED SAND AND TILL WITH THE SPECTRAL INDUCED POLARIZATION (SIP) METHOD. Geophysical Prospecting, **45**, no. 2,303-326.

Wang, M., S. Jin, M. Deng, W. Wei, and K. Chen. 2017, Multi-function electromagnetic transmitting system for mineral exploration. IEEE Transactions on Power Electronics, **PP**, no. 99,1-1.

Zhang, X., Q. Zhang, M. Wang, Q. Kong, S. Zhang, R. He, S. Liu, S. Li, and Z. Yuan. 2017, Development of a full-waveform voltage and current recording device for multichannel transient electromagnetic transmitters. Geoscientific Instrumentation Methods & Data Systems, **6**, no. 2,1-13.

Ziolkowski, A., R. Parr, D. Wright, V. Nockles, C. Limond, E. Morris, and J. Linfoot. 2010, Multi-transient electromagnetic repeatability experiment over the North Sea Harding field&Dagger. Geophysical Prospecting, **58**, no. 6,1159-1176.

Figures

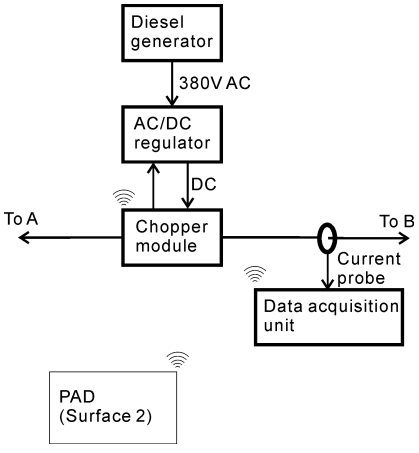

Geosci. Instrum. Method. Data Syst. Discuss., https://doi.org/10.5194/gi-2018-27
Manuscript under review for journal Geosci. Instrum. Method. Data Syst.
Discussion started: 2 January 2019

Geoscientific Instrumentation Methods and Data Systems Discussions
Open Access
EGU

Figure 1. Diagram of multifunction EM transmitter architecture (diesel generator, AC/DC regulator chopper module, current probe, data acquisition unit, cable, tablet computer (PAD))

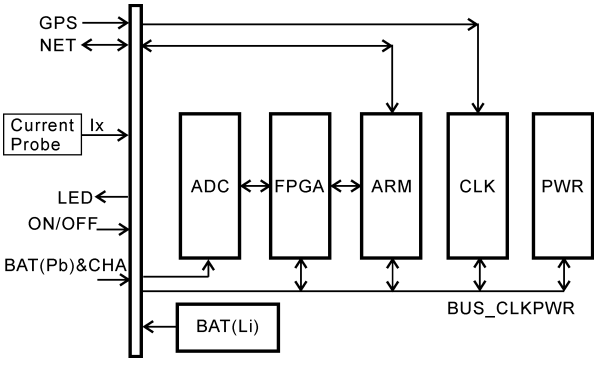

Figure 2 Block diagram of the current recorder

Figure 3. Photo of the data acquisition unit

Geosci. Instrum. Method. Data Syst. Discuss., https://doi.org/10.5194/gi-2018-27
Manuscript under review for journal Geosci. Instrum. Method. Data Syst.
Discussion started: 2 January 2019

Geoscientific Instrumentation Methods and Data Systems Discussions

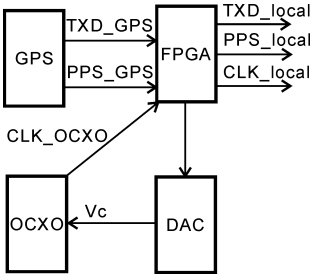

Figure 4. Block diagram of the clock module

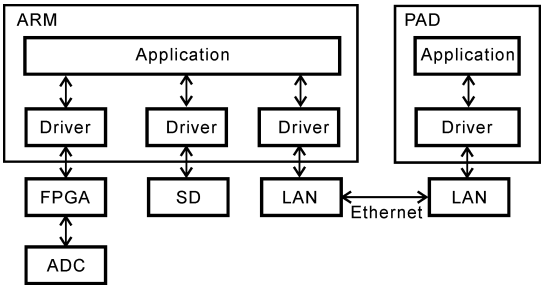

Figure 5. Data flow chart

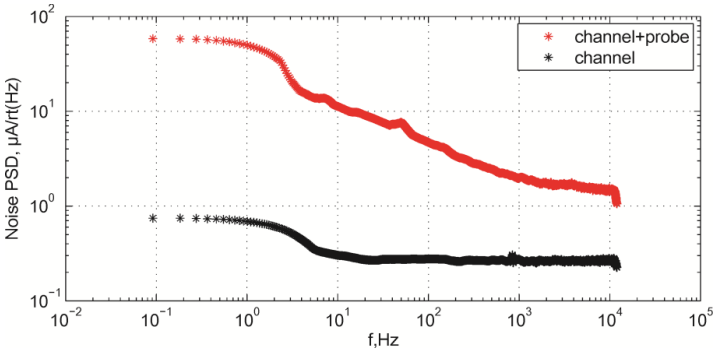

Figure 6. Current noise power spectrum density of the current probe and data acquisition unit obtained on a magnetic shield barrel

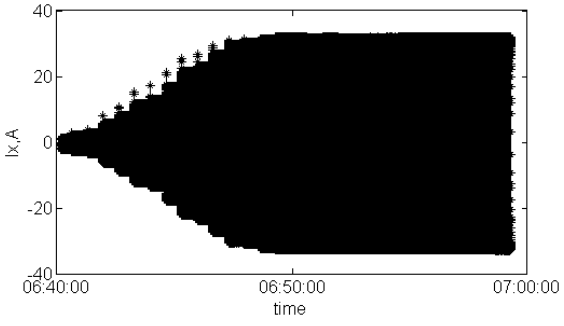

Geosci. Instrum. Method. Data Syst. Discuss., https://doi.org/10.5194/gi-2018-27
Manuscript under review for journal Geosci. Instrum. Method. Data Syst.
Discussion started: 2 January 2019

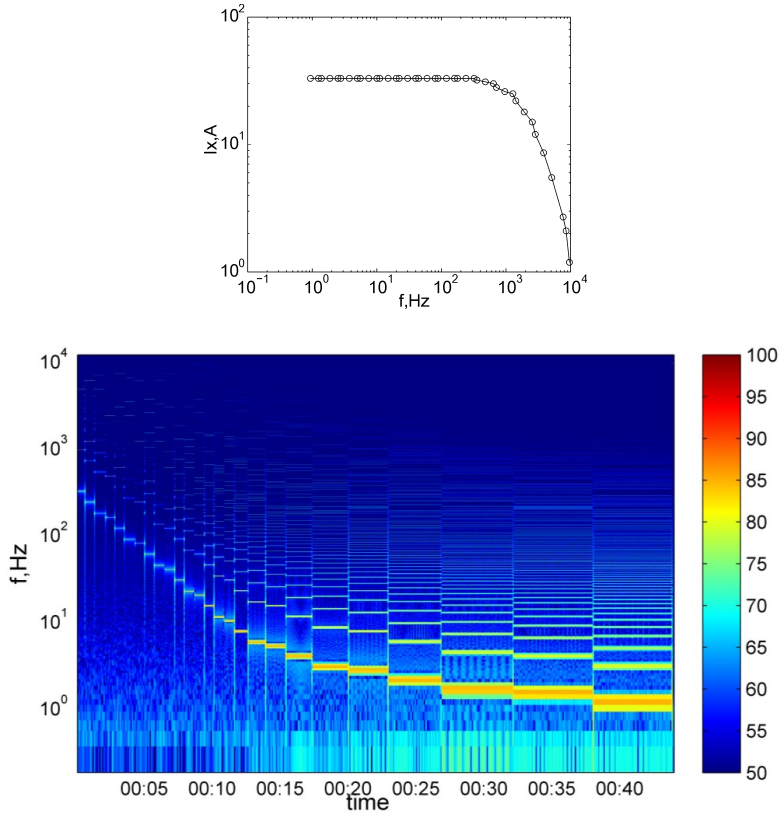

Figure 7a) Current time series as one complete cycle (CSAMT mode, duration 50 min, 9600 Hz to 0.9375 Hz, 2 Ap to 30 Ap); b) frequency stack result; and c) time frequency spectrum (CSAMT mode)

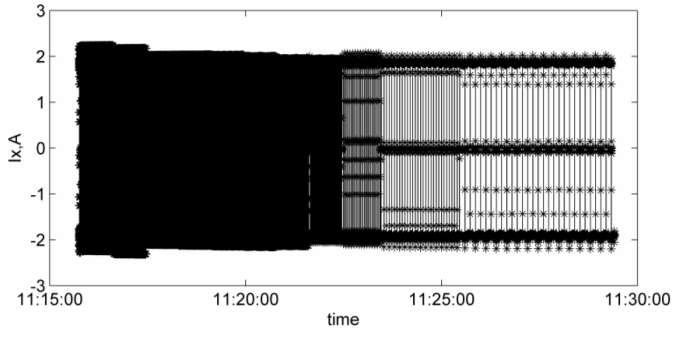

Geosci. Instrum. Method. Data Syst. Discuss., https://doi.org/10.5194/gi-2018-27
Manuscript under review for journal Geosci. Instrum. Method. Data Syst.
Discussion started: 2 January 2019

Geoscientific Instrumentation Methods and Data Systems Discussions

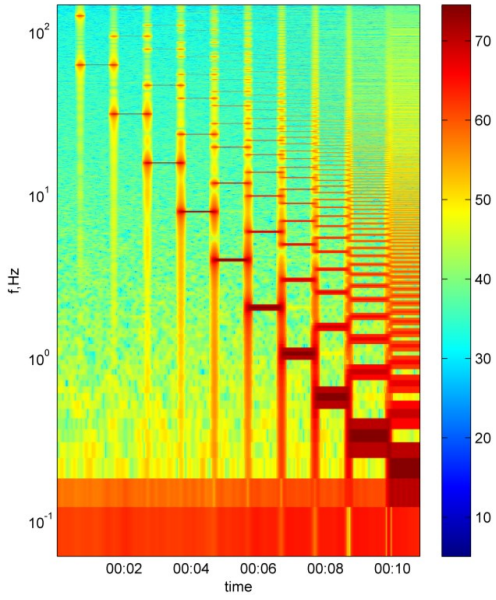

Figure 8 a) Raw current time series with whole circulation (15 min) and b) time frequency spectrum (SIP mode)

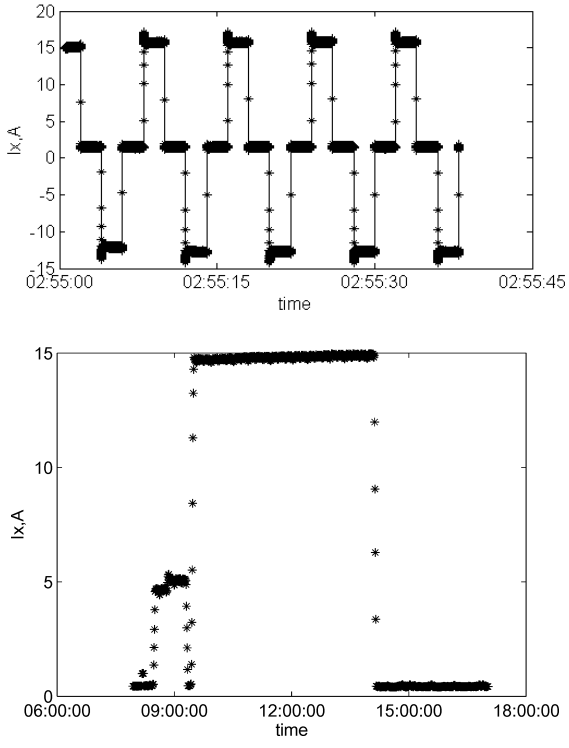

Figure 9 a) Current time series and b) Long time amplitude variable (TDIP mode)

Tables

Geosci. Instrum. Method. Data Syst. Discuss., https://doi.org/10.5194/gi-2018-27
Manuscript under review for journal Geosci. Instrum. Method. Data Syst.
Discussion started: 2 January 2019

Geoscientific Instrumentation Methods and Data Systems Discussions
Open Access
EGU

Table 1 Performance comparison of different current measurement solutions

Manufacture	IRIS	Phoenix	CUGB (Zhang, 2017)	CUGB (This paper)
Current transducer		CMU-1		A622
Current transducer principle		Hall effect sensor	Sample resistance	Hall effect sensor
Current recorder	I-FullWaver	RXU-TMR		EMR-CU
Transmitter	VIP-10000	TXU-30	MTEM	EMT48
Sample rate	100 Hz	10 kHz	32 kHz or 40 MHz	24 kHz
Sample mode	continuous	discontinuous	continuous	continuous
Precision	±3 mA		±1%	
Dynamic range			60 dB	97 dB
Input range	25 A	40 A	50 A	100 A
Advantage	full waveform, autonomous	integrated with transmitter controller	full waveform, voltage and current	full waveform, broad bandwidth, high precision
Disadvantage	bandwidth	discontinuous sample	accuracy & isolation	

Table 2. Performance comparison of different current transducers

Transducer	Sample resistance	Inductance mutual	Fiber	Hall effect sensor
Bandwidth	DC & AC	AC	DC & AC	DC & AC
Input range	Low	High	High	Middle
Sensitivity	High	Low	High	Middle
Isolation	No	Yes	Yes	Yes
Cost	Low	Middle	High	Low

5

Table 3. Specification of the current probe (A622 from Tektronix)

Specification	A622
Band width	DC to 100 kHz
Full scale	100 A peak
Sensitivity	10 mV/A or 100 mV/A

Termination	BNC
Maximum conductor diameter	11.8 mm

Table 4 Performance table compare with commercial current recorder from Phoenix geophysics

Performance	TMR-RXU (Phoenix geophysics)	This paper
Record mode	discontinuous	Full waveform record
Band width	DC to 10 kHz	DC to 10 kHz
Full scale input range	±40 A	±100 A
Dynamic range		97 dB
Noise level		10 μA/rt (Hz)@ 10 Hz
Storage	512 MB	32 GB
Time sync error	±0.5 μs	±0.1 μs